Low-Energy Impact Characterization Models and Damage Detection in Thin Monocoque Structures Using Artificial Intelligence

DANIEL DEL-RIO VELILLA, ANDRES PEDRAZA RODRIGUEZ, ANTONIO FERNANDEZ-LOPEZ
and ALFREDO GUEMES GORDO

ABSTRACT

The low damage tolerance of aircraft structures leads to an oversizing of their optimum weight as they are designed to withstand impacts on aerodynamic surfaces. Through the application of Structural Health Monitoring (SHM) techniques, which allow the characterization of impacts with a reduced number of sensors, further structural optimization is possible. This article proposes the use of Artificial Intelligence (AI) models for a complete impact characterization performed on an anisotropic Carbon Fibre Reinforced Plastic (CFRP) plate. The three principal objectives are impact location, characterization of the Impactor Object (IO), focusing on splitting the mass and velocity at equienergy impacts, and damage detection. The location task consists of the prediction of the impact coordinates (X-Y), while the energetic characterization of the IO predicts its mass, velocity, and energy when the impact occurs. These models are powered by low-cost piezoelectric (PZT) sensors, which acquire the acoustic wave generated by the impact, which allows the monitoring of large surfaces of complex geometry with a reduced number of sensors. These models have been trained with experimental data acquired with an Autonomous Impact Machine. This machine has performed more than 40,000 impacts on a coordinate grid that vary the IO mass, velocity, and impact energy, focusing on multiple equal energy combinations of the IO mass and impact velocity. Damage detection is performed by comparing the predictions of multiple location and characterization models.

INTRODUCTION

Composite materials in the aerospace industry have excellent mechanical properties but are vulnerable to low-energy impact damage such as cracks and delaminations [1]. The severity of damage depends on the impact energy, mass, and velocity of the object [2], leading to the deterioration of mechanical properties [3], and reduced service life due to fatigue [4]. Non-Destructive Inspection (NDI) techniques are used to assess damage

Daniel del-Rio Velilla, PhD Student, Email: daniel.delrio.velilla@upm.es. Center for Composite Material and Smart Structures (CCMSS), Department of Materials and Aerospace Manufacturing, Escuela Tecnica Superior de Ingenieria Aeronautica y del Espacio, Universidad Politecnica de Madrid, Madrid, Spain

severity but require prior localization.

Various methods for impact localization in composite structures exist. Most studies focus on low-curvature exterior structures, such as aerodynamic surfaces, using flat panels with or without stiffeners. Sensors such as PZT sensors [5] or combinations of accelerometer-fiber optic sensors [6] are used for impact localization, often employing time-of-arrival techniques in simple structures.

Impact energy is classified into subcritical, delamination, and fiber fracture levels [7]. Energy estimation helps determine if manual inspection is necessary. The influence of IO mass and velocity on damage generation has been studied, with models relating energetic parameters to damage type [8]. Velocity affects energy absorption, resulting in a wider damage range at higher velocities. It is important to identify the combinations of mass and velocity that cause the impact [7].

AI algorithms are replacing traditional techniques in Structural Health Monitoring, particularly in complex composite structures, due to their ability to locate and characterize impacts with reduced errors [9]. However, previous studies focused on simple structures without stiffeners and used simulations or insufficient experimental data for training. Convolutional Neural Networks have shown success in impact energy classification [10].

This work demonstrates impact location and characterization feasibility using Deep Learning (DL) models. DL models separate the energy, mass, and velocity parameters of the impacting object. A database of real free fall impacts, generated using an Autonomous Impactor, provides a large number of experimental samples with accurate labeling with which the models had been trained. Results and conclusions will be presented on the basis of the analysis of the trained models, and a damage detection technique will be presented.

SPECIMEN UNDER STUDY, TEST CONFIGURATION AND EXPERIMENTAL DATA ACQUISITION

The specimen selected is a flat CFRP plate stiffened by a T beam made of unidirectional prepreg with quasi-isotropic stacking. Plate dimensions are $577.3 \times 577.3 \times 2\ \mathrm{mm}^3$. The reference system of the plate has the X axis perpendicular to the stiffener, the Y axis parallel to it, and the Z axis forming a right trihedron. This sample has eight PZT (7BB-20-3 PZT) sensors attached to its surface to acquire the acoustic wave generated by the impact. In Figure 1 the numbering of the sensors is presented.

The boundary conditions applied to the specimen are as follows. The two plate edges parallel to Y-axis were clamped to two 4040 extruded aluminum profiles and these profiles were clamped to a structure thus restricting all its degrees of freedom. The other two sides, the X-axis, were left free.

In order to use a Deep Neural Network (DNN) tool, a large impact data set needs to be generated. This database shall contain impacts at different coordinates on the plate with an IO of variable mass and which can be dropped from different heights achieving different impact velocities, therefore, different energies.

The spatial discretization of the surface consists of a grid of points resulting from dividing the total length of the surface by the diameter of the tube (43.2 mm) through

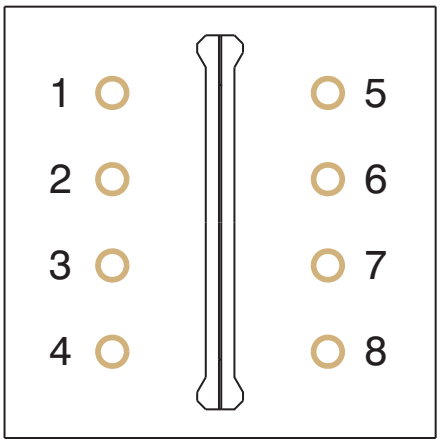

Figure 1. Plate scheme.

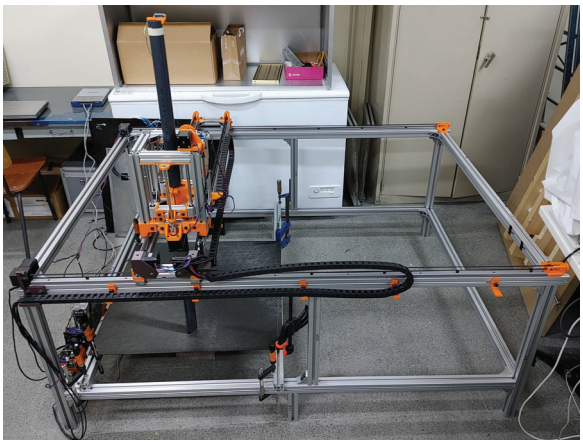

Figure 2. Autonomous Impact Machine.

which the IO falls, giving a total of 12×14 impact points.

Energy discretization consists of generating a data set with impacts in which the IO has different masses, impact velocities, and energies. Impacting at different masses is achieved by adding calibrated steel discs to the IO. The different impact velocities are obtained by dropping the IO from different heights, as the impacts are made by free fall. To transform the drop height into impact velocity, the equations for the kinetic and potential energy have been equated, and the velocity has been cleared. However, an energy value can be achieved with multiple combinations of mass and velocity, and an essential task of the model will be to separate these two possible combinations.

The IO mass values start at 75 grams and increase by 10 grams to 175, making a total of 11 different masses. The lowest height at which impacts were made was 35 mm and increased by 7.5 mm to 260, for a total of 31 different heights. For each mass, impacts were made at all coordinates and at all release heights, exceeding 48,500 impacts in total.

Obtaining such a high number of experimental impacts was possible thanks to the use of an Autonomous Impact Machine (AIM), Figure 2. AIM can perform impacts in a total volume of $1,440 \times 990 \times 150$ mm^3. The maximum mass of IO that it can move is 1 kg and the maximum release height is 2 m, reaching an impact energy of 19.62 J. The AIM performs the impacts by turning off an electromagnet and dropping the IO. At the same time, it starts the acquisition process and stores the impact, checked, and labeled in the computer.

Artificial intelligence models cannot be fed data directly from sensors, the acquired samples need to be processed. Therefore, the acquired impacts have been reduced to a total length of 2,000 samples per sensor, 16,000 per impact, with a total duration of 16 ms. The normalization has then been applied to all impacts, where the maximum and minimum values used are shown in Table I.

TABLE I. Normalization values.

Operator	**PZT [V]**	**X [mm]**	**Y [mm]**	**m [g]**	**v [m/s]**	**E [mJ]**
min	-12.4	0	0	75	0	40
max	12.4	500	500	175	1	400

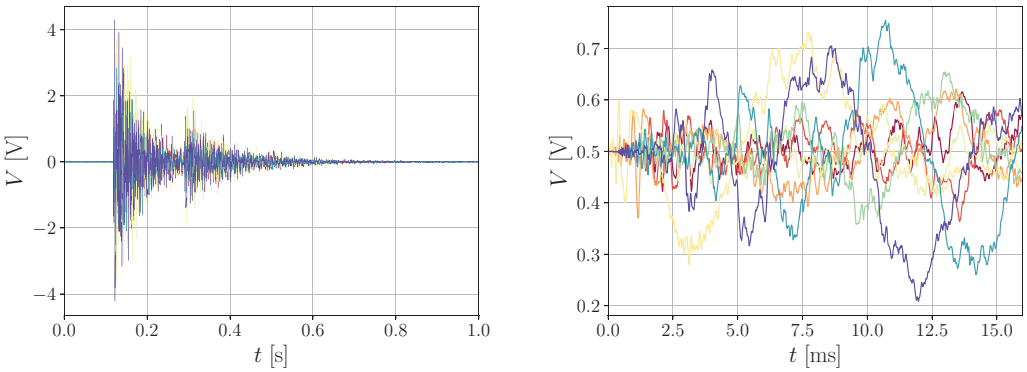

(a) Raw impact.

(b) Processed impact.

Figure 3. Comparison of an impact before and after it has been processed.

A comparison of an impact before and after trimming and normalizing is shown in Figure 3.

MODEL ARCHITECTURE AND METRICS DEFINITION

The architecture of the models that define the location and energy characterization of an impact is the same. A high-level block diagram of the architecture is shown in Figure 4a. The architecture consists of two distinct stages. The first stage (dark blocks) is responsible for compressing the acoustic waves collected by the PZTs and generating a new vector with the compressed information; its mission is to extract the most important features of the impact. This vector is the input of the second stage (gray blocks) in which independent regressions of the parameters are performed, returning a vector of $1 \times N$, where N is the number of impact parameters predicted by the model.

The internal structure of the trapezoidal blocks consists of a set of layers that are stacked by progressively reducing the number of neurons, Figure 4b. The number of layers in each block and its number of neurons are set by the parameters *compFE*, *outFE*, and *comReg*. The values used in this work are 200, 150, and 100 respectively.

The two models developed are based on the same architecture described above. Both models have a total of eight FE blocks as 8 PZTs are used; however, the Locator model has only two regression blocks (X and Y) compared to three (m, v and E) for the Characterizer model.

The preprocessed data set has been divided four times into three groups (*training*-40%, *validation*-20% and *test*-20% randomly) to perform the k-Cross Validation.

The presented model is a regressor, so it returns a continuous and normalized prediction of each variable. Each predicted variable has an associated error with respect to its target value,

$$NE_{\mathrm{i,j}} = \hat{Y}_{\mathrm{i,j}} - \hat{y}_{\mathrm{i,j}}\,, \tag{1}$$

where $\hat{Y}_{\mathrm{i,j}}$ is the normalized j target of the impact i, and the $\hat{y}_{\mathrm{i,j}}$ is the prediction of the model.

The metric used to assess the performance of the models will be the percentage

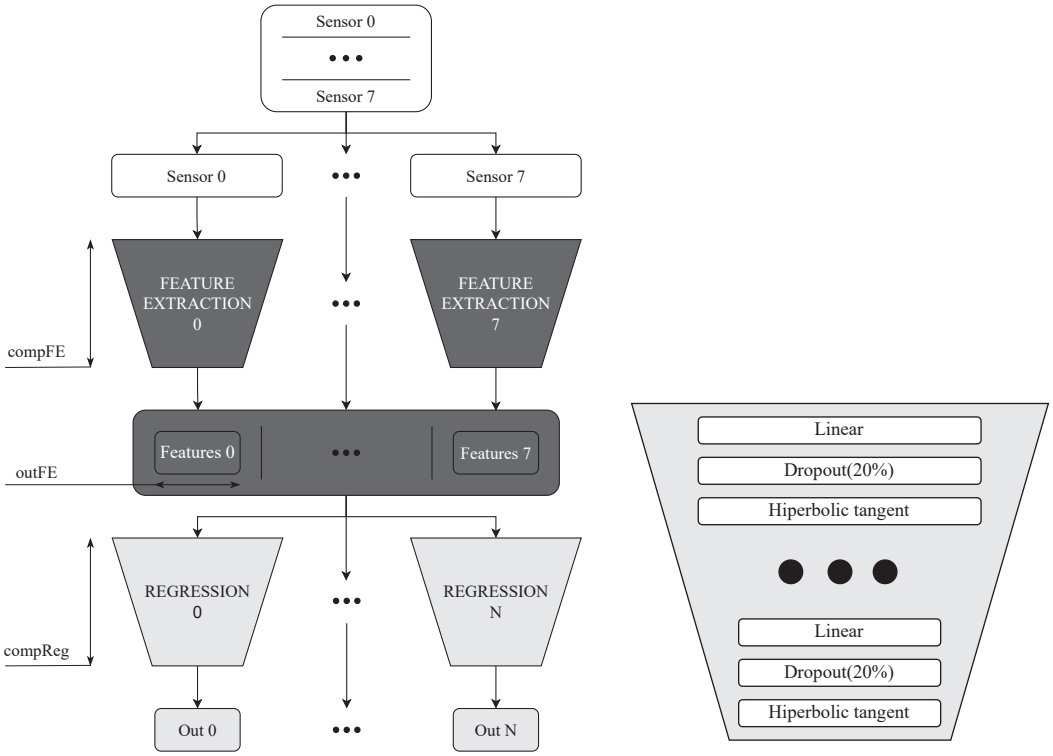

(a) Artificial Intelligence Tool architecture. (b) Low level block detail.

Figure 4. Model architecture block diagram.

Normalized Euclidean Error, NEE, calculated as

$$NEE_{\mathrm{i}} = \sqrt{\sum_{\mathrm{j=1}}^{\mathrm{k}} NE_{\mathrm{i,j}}^2} \times 100\,, \tag{2}$$

where k is the model's total number of outputs, i is the current impact, and j corresponds to a given target. This magnitude gives an idea of the error distance as a combination of all variables.

LOCATOR AND CHARATERIZER RESULTS

Once the models have been trained, the results of the four distributions for the locator and characterizer models are presented. The models that have generated the results shown in this section have been trained with all sensors embedded in the structure.

Figure 5 shows the mean and standard deviation of NEE for each of the random distributions of the impacts. On the other hand, Figure 6 shows the histogram with the NEE values of the model that has obtained the best metrics.

DAMAGE DETECTION

To simulate damage to the structure, vacuum sealant was glued to the surface where

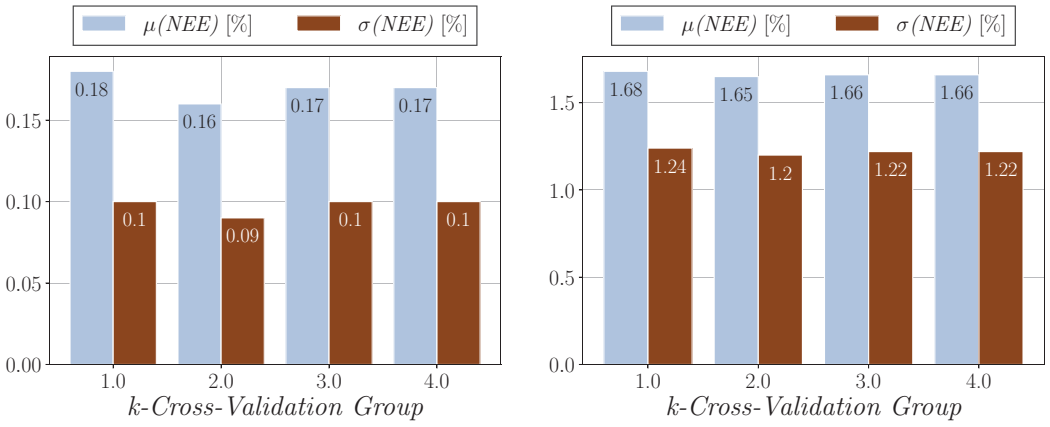

(a) Locator model. (b) Characterizer model.

Figure 5. k-Cross Validation results.

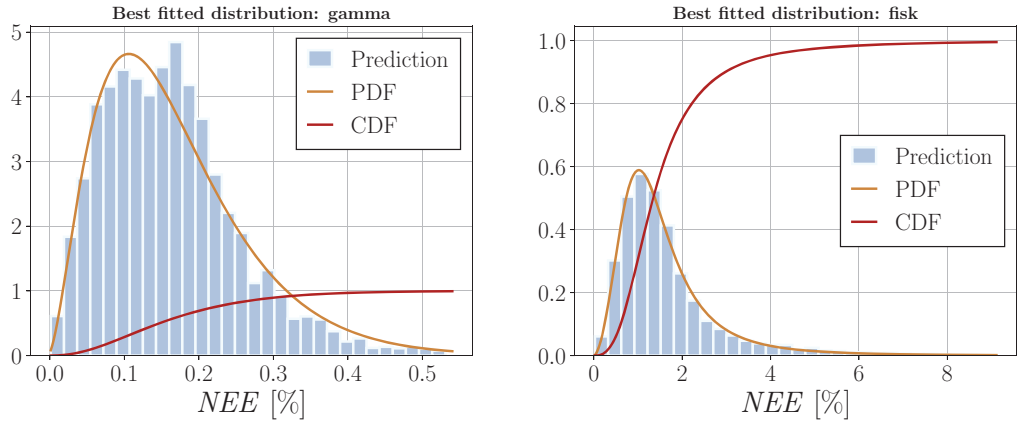

(a) Locator model. (b) Characterizer model.

Figure 6. NEE histograms of the best-trained models.

the stiffener is located. Three rounds of impacts were performed with a mass of 75 grams and at the same heights as previously described, however, in each round the vacuum sealant was in a different position. A total of 13,299 impacts were acquired with the damaged structure.

The proposed damage detection technique is based on the confidence in the predictions of trained models with the undamaged structure, the confidence being the probability value 99% of the NEE CDF curve, $NEE_{99\%}$, shown in Figure 6.

The procedure consists of comparing the distance between two models' predictions of the same impact. As there is confidence that the model **i** will make a prediction with a NEE of less than $NEE_{99\%,\mathrm{i}}$, if the distance between the model **i** and **j** exceeds the value $NEE_{99\%,\mathrm{i}}$, the structure is considered damaged. If, on the other hand, the prediction is at a distance of less than $NEE_{99\%,\mathrm{i}}$, the structure is considered to be undamaged.

The results shown below correspond to two combinations of four models. The first combination has been fed with only one sensor per model, C1, while the second has

TABLE II. $NEE_{99\%}$ values for C1 of sensors.

Variable	Sensors in model			
	[0]	**[3]**	**[4]**	**[7]**
m	11.43	11.68	11.77	11.03
v	4.85	5.02	4.95	4.71
E	4.5	4.48	4.51	4.38
mvE	12.09	12.74	12.76	12.05
X	3.97	3.91	4.77	4.76
Y	4.24	3.65	4.34	3.41
XY	4.91	4.93	5.37	5.04

TABLE III. Damage detection results [%] for the C1 combination.

Variable	Dam		Und	
	Dam	**Und**	**Dam**	**Und**
m	94.84	1.2	5.16	98.8
v	92.63	1.46	7.37	98.54
E	78.74	2.53	21.26	97.47
mvE	**97.37**	1.06	2.63	**98.94**
X	75.98	8.4	24.02	91.6
Y	71.55	8.58	28.45	91.42
XY	89.5	10.36	10.5	89.64

TABLE IV. $NEE_{99\%}$ values for C2 of sensors.

Variable	Sensors in model			
	[0, 4]	**[4, 7]**	**[7, 3]**	**[3, 0]**
m	9.96	9.23	9.37	9.29
v	3.39	3.16	3.19	3.33
E	3.62	3.4	3.42	3.39
mvE	12.27	11.08	11.38	11.18
X	2.45	2.37	2.22	1.78
Y	2.4	1.96	1.81	1.8
XY	2.87	2.73	2.58	2.17

TABLE V. Damage detection results [%] for the C2 combination.

Variable	Dam		Und	
	Dam	**Und**	**Dam**	**Und**
m	91	0.69	9	99.31
v	**93.41**	1.42	6.59	98.58
E	70.52	1.15	29.48	98.85
mvE	92.92	0.35	7.08	**99.65**
X	74.14	7.14	25.86	92.86
Y	77.02	6.95	22.98	93.05
XY	93.02	9.19	6.98	90.81

used two, C2. Tables II and IV show the values of $NEE_{99\%}$ for each of the variables predicted by the model, in addition to the overall prediction combination. Tables III and V show first the results of the classification of impacts on the damaged structure and then on impacts on the undamaged structure. In this way, the error of predicting the presence of damage when there is no damage and vice versa can be appreciated.

CONCLUSIONS

The models shown demonstrate that both the location of the position of an impact and the energetic characterization of the impact are possible by using Artificial Intelligence. Although the localization model has higher precision than the energy characterizer, the mean values NEE are equal to or below the unity per cent. In addition, confidence in the predictions of the model has allowed the generation of a structural health classifier that detects 99% that there is no damage to a healthy structure and 97% that there is damage to a damaged structure.

ACKNOWLEDGEMENT

This project has received funding from the national research program Retos de la Sociedad under the Project STARGATE: Desarrollo de un sistema de monitorización

estructural basado en un microinterrogador y redes neuronales (reference PID2019-105293RB-C21)

REFERENCES

1. Davies, G. A. O. and R. Olsson. 2004. "Impact on composite structures," *THE AERONAUTICAL JOURNAL*:541–563, doi:10.1017/s0001924000000385.
2. Aryal, B., E. V. Morozov, H. Wang, K. Shankar, P. J. Hazell, and J. P. Escobedo-Diaz. 2019. "Effects of impact energy, velocity, and impactor mass on the damage induced in composite laminates and sandwich panels," *Composite Structures*, 226, ISSN 02638223, doi:10.1016/J.COMPSTRUCT.2019.111284.
3. Pavier, M. J. and M. P. Clarke. 1995. "Experimental techniques for the investigation of the effects of impact damage on carbon-fibre composites," *Composites Science and Technology*, 55:157–169, ISSN 0266-3538, doi:10.1016/0266-3538(95)00097-6.
4. Tai, N. H., M. C. Yip, and J. L. Lin. 1998. "Effects of low-energy impact on the fatigue behavior of carbon/epoxy composites," *Composites Science and Technology*, 58:1–8, ISSN 02663538, doi:10.1016/S0266-3538(97)00075-4.
5. Zhou, J., V. J. Mathews, and D. O. Adams. 2019. "Acoustic emission–based impact location estimation on composite structures," *https://doi.org/10.1177/1475921718820521*, 18:1652–1668, ISSN 17413168, doi:10.1177/1475921718820521.
6. Frieden, J., J. Cugnoni, J. Botsis, and T. Gmür. 2012. "Low energy impact damage monitoring of composites using dynamic strain signals from FBG sensors - Part I: Impact detection and localization," *Composite Structures*, 94:438–445, ISSN 02638223, doi:10.1016/J.COMPSTRUCT.2011.08.003.
7. Zabala, H., L. Aretxabaleta, G. Castillo, J. Urien, and J. Aurrekoetxea. 2014. "Impact velocity effect on the delamination of woven carbon-epoxy plates subjected to low-velocity equienergetic impact loads," *Composites Science and Technology*, 94:48–53, ISSN 02663538, doi:10.1016/J.COMPSCITECH.2014.01.016.
8. Chai, G. B. and S. Zhu. 2011. "A review of low-velocity impact on sandwich structures," *Proceedings of the Institution of Mechanical Engineers, Part L: Journal of Materials: Design and Applications*, 225:207–230, ISSN 1464-4207, doi:10.1177/1464420711409985.
9. Malekloo, A., E. Ozer, M. AlHamaydeh, and M. Girolami. 2022. "Machine learning and structural health monitoring overview with emerging technology and high-dimensional data source highlights," *Structural Health Monitoring*, 21:1906–1955, ISSN 1475-9217, doi:10.1177/14759217211036880.
10. Damm, A. M., C. Spitzmüller, A. T. S. Raichle, A. Bühler, P. Weißgraeber, and P. Middendorf. 2020. "Deep learning for impact detection in composite plates with sparsely integrated sensors," *Smart Materials and Structures*, 29:125014, ISSN 0964-1726, doi:10.1088/1361-665X/abb644.